

# The Impact of Wettability on the Co-moving Velocity of Two-Fluid Flow in Porous Media

Fatimah Alzubaidi<sup>1</sup> · James E. McClure<sup>2</sup> · Håkon Pedersen<sup>3</sup> · Alex Hansen<sup>3</sup> · Carl Fredrik Berg<sup>4</sup> · Peyman Mostaghimi<sup>1</sup> · Ryan T. Armstrong<sup>1</sup>

Received: 9 October 2023 / Accepted: 17 May 2024 / Published online: 5 July 2024 © The Author(s) 2024

#### Abstract

The impact of wettability on the co-moving velocity of two-fluid flow in porous media is analyzed herein. The co-moving velocity, developed by Roy et al. (Front Phys 8:4, 2022), is a novel representation of the flow behavior of two fluids through porous media. Our study aims to better understand the behavior of the co-moving velocity by analyzing simulation data under various wetting conditions. We analyzed 46 relative permeability curves based on the Lattice-Boltzmann color fluid model and two experimentally determined relative permeability curves. The analysis of the relative permeability data followed the methodology proposed by Roy et al. (Front Phys 8:4, 2022) to reconstruct a constitutive equation for the co-moving velocity. Surprisingly, the coefficients of the constitutive equation were found to be nearly the same for all wetting conditions. On the basis of these results, a simple approach was proposed to reconstruct the relative permeability of the oil phase using only the co-moving velocity relationship and the relative permeability of the water phase. This proposed method provides new information on the interdependence of the relative permeability curves, which has implications for the history matching of production data and the solution of the associated inverse problem. The research findings contribute to a better understanding of the impact of wettability on fluid flow in porous media and provide a practical approach for estimating relative permeability based on the co-moving velocity relationship, which has never been shown before.

**Keywords** Co-moving velocity  $\cdot$  Relative permeability  $\cdot$  Digital rock  $\cdot$  Wettability  $\cdot$  Multiphase flow

<sup>&</sup>lt;sup>4</sup> PoreLab, Department of Geoscience and Petroleum, Norwegian University of Science and Technology, Trondheim, Norway



Ryan T. Armstrong ryan.armstrong@unsw.edu.au

School of Civil and Environmental Engineering, The University of New South Wales, Sydney, Australia

National Security Institute, Virginia Tech, Blacksburg, VA, USA

<sup>&</sup>lt;sup>3</sup> PoreLab, Department of Physics, Norwegian University of Science and Technology, Trondheim, Norway

## 1 Introduction

The phenomenological two-phase extension of Darcy's law was proposed by Wyckoff and Botset (1936). The conceptual idea was that during flow, the presence of one fluid occludes the movement of the other fluid, and vice versa. The concept of relative permeability captures this behavior by defining how permeable a medium is to a given fluid on the basis of its saturation. The concept of "how permeable" is measured relative to the permeability of the medium for single-phase flow. The prevalence and longevity of the two-phase extension of Darcy's law in the porous media community speaks to its usefulness and simplicity. Here, we explore a thermodynamic framework provided by Hansen et al. (2018) that is compatible with the two-phase extension of Darcy's law but provides (1) new insights into the transport behavior of immobile phases in porous media and (2) a new capability for constructing relative permeability curves that has never been shown before.

The theory presented by Hansen et al. (2018) provides a fresh perspective on the "kinematics" of multiphase flow in the sense that the theory is only concerned with relationships between the velocities of the fluids. Fluid velocities are the seepage velocity, i.e., the average pore velocity, of each fluid,  $v_w = q_w/(\phi S_w)$  and  $v_n = q_n/(\phi S_n)$ , where the subscripts w and n refer to the wetting fluid and the non-wetting fluid, respectively, q is the volumetric flux, S is the saturation, and  $\phi$  is the porosity. We define the total seepage velocity as

$$v_p = S_w v_w + S_n v_n, \tag{1}$$

where  $S_w + S_n = 1$  are the saturations. The *co-moving velocity* is defined as

$$v_m = S_w \frac{\mathrm{d}v_w}{\mathrm{d}S_w} + S_n \frac{\mathrm{d}v_n}{\mathrm{d}S_w},\tag{2}$$

see Hansen et al. (2018), Feder et al. (2022), Roy et al. (2022), Pedersen and Hansen (2023) for further details. Hence, the co-moving velocity is the saturation-weighted average of the seepage velocity rate of change of each fluid under saturation change. These two equations may be inverted to give

$$v_w = v_p + S_n \left[ \frac{\mathrm{d}v_p}{\mathrm{d}S_w} - v_m \right],\tag{3}$$

and

$$v_n = v_p - S_w \left[ \frac{\mathrm{d}v_p}{\mathrm{d}S_w} - v_m \right]. \tag{4}$$

Therefore, knowing the total seepage velocity  $v_p$  and the co-moving velocity  $v_m$ , we find the seepage velocity for each fluid. The four equations constitute a two-way mapping between the pairs  $(v_w, v_n)$  and  $(v_p, v_m)$ . This mapping is concerned only with the relationship between the fluid seepage velocities. While the development of specific flow regimes would indeed influence the seepage velocities measures, the mapping is not influenced. The theory therefore provides a new frame of reference at the continuum scale that is fundamental.

By taking the derivative of the total seepage velocity  $v_p$  with respect to the wetting saturation  $S_w$  in Eq. 1, and combining the result with the definition of the co-moving velocity in Eq. 2, we find the expression



$$\frac{\mathrm{d}v_p}{\mathrm{d}S_w} = v_w - v_n + v_m,\tag{5}$$

demonstrating that the co-moving velocity is related to the velocity difference between the two fluids. Intuitively, the flow of each fluid carries along some of the other fluid. In addition, the cluster structure of two immiscible fluids can interact with the porous medium. The degree to which these two effects occur is captured by the co-moving velocity. Roy et al. (2020) provides further information on the physical origin of the co-moving velocity.

The co-moving velocity has been studied for various porous systems (Roy et al. 2022) and was found to follow a simple functional form,

$$v_m = av_0 + b \frac{\mathrm{d}v_p}{\mathrm{d}S_{..}},\tag{6}$$

where  $v_0$  is a velocity scale.

From Eqs. 5 and 6,

$$v_n - v_w = av_0 + (b-1)\frac{dv_p}{dS_w},$$
 (7)

the linear relationship is seen as a consequence of the velocity difference between the flowing fluids. The co-moving velocity relates the seepage velocities of the two competing fluids within a given porous medium.

The linear relationship (Eqs. 7 or 6) has been demonstrated for a wide range of Capillary numbers and Mobility ratios (Roy et al. 2022). Remarkably, the co-moving velocity relationship remains linear even when the total seepage velocity relationship becomes non-linear (Roy et al. 2022). Hansen et al. (2023) showed why  $dv_p/dS_w$  is the natural variable for  $v_m$ . However, it remains an open question as to why the co-moving velocity takes such a simple affine form. The co-moving velocity was first formulated in a thermodynamic-like description of two-phase flow in porous media Hansen et al. (2018). In the mathematical structure of thermodynamics, the linear relation of the co-moving velocity is possible, but such a simple relationship is not required and is not necessarily expected by the known physics. We speculate that this relationship is a consequence of partitioning the system into two separate fluid systems. However, further theoretical work is required to validate this speculation. Nevertheless, exploring the co-moving velocity relationship with experimental and simulation data will provide further insights that can guide the development of the theory, which is the aim of this paper.

The wetting state of a porous medium is an important factor that influences the geometric state of the fluids and therefore the relative permeability (Anderson 1986, 1987; Masalmeh 2003). The geometric state of a fluid is defined by Minkowski functionals, which provide a unique set of geometrical measures (McClure et al. 2018; Armstrong et al. 2019). Studying the co-moving velocity under different wetting conditions is a logical step to unravelling the linearity of the co-moving velocity relationship. On the pore scale, the geometric arrangement of the fluids depends on local wetting conditions, which affects the surface area coverage (Garfi et al. 2020), the Gaussian curvature (Lin et al. 2019), and the mean curvature (Lin et al. 2018) of the fluids. The energy required to move an interface also decreases when the surface energies between fluids and solid are similar, i.e., near a contact angle of 90 degrees (Armstrong et al. 2021). Therefore, the propensity for interfacial rearrangements and intermittency increases under intermediate wet conditions,



resulting in complex interactions between flowing fluids (Reynolds et al. 2017; Lin et al. 2021; Scanziani et al. 2020). It is therefore reasonable to assume that wettability would impact the co-moving velocity relationship in unexpected ways.

Herein, we investigate the impact of wettability on the constitutive relationship for the co-moving velocity, i.e., Eq. 6. For our analyses, we rely on previously published relative permeability curves. Firstly, relative permeability simulations for a range of different wetting conditions are analyzed to investigate the co-moving velocity relationship. The simulation data are based on two different rock types under a range of different wetting conditions, which have been published elsewhere (Al-Zubaidi et al. 2023). Secondly, we substantiate our result based on the simulation data by using experimental core flooding data from Zou et al. (2018). Lastly, we demonstrate a practical application by reconstructing full relative permeability curves when only the relative permeability of a single phase and its co-moving velocity relationship are known.

## 2 Materials and Methods

Firstly, we will explain the theoretical developments used in this paper. We will then briefly explain the relative permeability data used for our analysis. The relative permeability curves used for our analyzes have been published elsewhere. Relevant publications are McClure et al. (2021), Zou et al. (2018), Al-Zubaidi et al. (2023).

## 2.1 Co-moving Velocity and Relative Permeability

Two-phase Darcy law for the seepage (i.e., average pore) velocities, when there are no saturation gradients present, is expressed as follows:

$$v_i = \frac{k_{ri}\mathsf{K}}{\phi S_i \mu_i} |\nabla p|,\tag{8}$$

where the usual minus sign is combined with the negative gradient to produce a positive number, expressed as  $|\nabla p|$ . Furthermore,  $k_{ri}$  is the relative permeability of phase i,  $\mu_i$  is the viscosity of phase i,  $\phi$  is the porosity, K is the absolute permeability, and p is pressure. It should be noted that (1) the simulated data used were conducted at steady state with no saturation gradients and (2) the experimental data used was conducted at steady state with capillary-end effect correction through history matching.

The co-moving velocity can be directly determined from the relative permeability. From Eqs. 5 and 8,

$$v_m/v_0 = \frac{d(v_p/v_0)}{dS_w} + \mu_w \left[ \frac{k_{rn}}{\mu_n S_n} - \frac{k_{rw}}{\mu_w S_w} \right]. \tag{9}$$

where

$$v_p/v_0 = \mu_w \left[ \frac{k_{rw}}{\mu_w} + \frac{k_{rn}}{\mu_n} \right]. \tag{10}$$

We define a velocity scale that must be positive,



$$v_0 = \frac{\mathsf{K}}{\mu_w \phi} |\nabla p|. \tag{11}$$

Our analysis is based on the produced relationship between  $v_p/v_0$  versus  $S_w$ ,  $v_m/v_0$  versus  $S_w$ , and  $v_m/v_0$  versus  $d(v_p/v_0)/dS_w$ . The latter represents the constitutive relationship for the co-moving velocity as given in Eq. 6. These relationships will be determined in Sect. 3.1 where it should be noted that, based on Eqs. 8–11, the relative permeability curves are the only data required for the analysis.

Lastly, the Corey model for relative permeability will be used in Sect. 3.3 of the results. The Corey model is commonly used to approximate the functional relationship between the relative permeability and saturation,

$$k_{\rm rn} = k_{\rm rn,max} \left( \frac{1 - S_w - S_{\rm nr}}{1 - S_{\rm iw} - S_{\rm nr}} \right)^{\eta_o}$$
 (12)

$$k_{\rm rw} = k_{\rm rw,max} \left( \frac{S_w - S_{\rm iw}}{1 - S_{\rm iw} - S_{\rm nr}} \right)^{\eta_w},$$
 (13)

where  $S_{\rm iw}$  is irreducible wetting phase saturation,  $S_{\rm nr}$  is residual non-wetting phase saturation,  $k_{\rm rn,max}$  is the maximum non-wetting phase relative permeability, and  $k_{\rm rw,max}$  is the maximum wetting phase relative permeability.

## 2.2 Simulated Relative Permeability Data

We used previously published relative permeability curves simulated with a parallel implementation of the color-gradient Lattice–Boltzmann method. The code has been documented and validated elsewhere and allows for spatially varied wetting conditions on a per-voxel basis McClure et al. (2021). The simulation domains were North Sea sandstone and Bentheimer sandstone. In the following subsections, the salient points regarding the domains and simulation settings are explained. Full simulation details are provided in the original publications Al-Zubaidi et al. (2023), McClure et al. (2021).

## 2.2.1 North Sea Sandstone

The North Sea sandstone had porosity and permeability of 23% and 640 mD, respectively. The simulation domain was generated by coupling micro-CT images with scanning Electron Microscopy Energy Dispersive Spectroscopy (SEM-EDS) followed by Quantitative Evaluation of Materials by Scanning Electron Microscopy (QEMSCAN) software. The result provided a full three-dimensional image of the pore structure and mineralogy at 2.3  $\mu$ m micrometer resolution. The total image size was  $1000 \times 1000 \times 750$  voxels. For simplicity, the minerals identified by QEMSCAN were categorized into three main groups: quartz, carbonate, and clay for wettability assignment.

Wettability was controlled by changing the contact angle, which at equilibrium relates to various surface energies in the two-fluid system as defined by Young's equation. These surface energies can be assigned to the solid surface domain on a per voxel basis McClure et al. (2021). The wettability was distributed four ways.

1. Homogeneous Wet: same condition on the entire grain surface.



Corner Wet: oil is injected based on a morphological approach to achieve irreducible water saturation. Parts of the grain surface that touch oil get their own wetting condition, while corners remain water wet.

- 3. Heterogeneous Wet: each mineral type gets a different wettability.
- Heterogeneous-Corner Wet: combination of 2 and 3.

The domain wettability was defined by summation of the cosine of the contact angles for each mineral/fluid/fluid pair, determined as

$$W = (\gamma_{qn} - \gamma_{qw})/\gamma_{wn}\phi_q + (\gamma_{kn} - \gamma_{kw})/\gamma_{wn}\phi_k + (\gamma_{cs} - \gamma_{cs})/\gamma_{wn}\phi_c, \tag{14}$$

where  $\phi_q$ ,  $\phi_k$  and  $\phi_c$  are the solid voxel fractions of quartz, clay, and carbonate, respectively. This metric provides a scale from strongly water-wet (W = 1.0) to strongly oil-wet (W = -1.0).

The simulated fluids had the same viscosity and the Capillary number was approximately  $10^{-5}$  for all simulations. The Capillary number is defined as:  $Ca = (\mu_w v_w + \mu_n v_n)/\gamma_{wn}$ . The simulations were conducted in steady-state mode under water flooding, in which any phase leaving the outlet was introduced to the inlet to keep fractional flow and saturation constant until the simulation converged. The full details of LBPM's 'steady-state' protocol are explained in McClure et al. (2021). Such requirements do not allow for the development of a saturation gradient nor saturation fluctuations. The convergence criterion was based on stabilization of the Capillary number McClure et al. (2021).

#### 2.2.2 Bentheimer Sandstone

The Bentheimer sandstone had porosity and permeability of 24% and 1.3 D, respectively. The simulation domain was generated by micro-CT only and thus did not contain any mineralogical information. The pore structure was imaged at a resolution of 1.66  $\mu$  micrometers. The resulting image size was  $900 \times 900 \times 1600$  voxels. The results of these simulations are unique to this publication, but utilize the same method as published in McClure et al. (2021), Al-Zubaidi et al. (2023). For Bentheimer sandstone only Type 2 wettability was used. The simulation settings were the same as those used for the North Sea sandstone, i.e., Capillary number, viscosity, boundary conditions, and convergence criteria.

#### 2.3 Experimental Relative Permeability Data

We used experimental relative permeability data from Zou et al. (2018). Full details on how relative permeability was measured are provided by Zou et al. (2018), while the salient points for the co-moving velocity analysis are provided below.

Zou et al. (2018) conducted core flooding studies using a mini-core plug of Bentheimer sandstone. The sample had a porosity and permeability of 24% and 2.54 D, respectively. The core was 18.5 mm long with a diameter of 10.2 mm. The fluids were decane and water. Relative permeability was first measured in the core under its clean water-wet state. The core was then treated with octadecytrichlorosilane (OTS), while connate water was frozen in the corners of the pores. OTS rendered the exposed core surfaces oil wet with an estimated contact angle of 115° based on the resulting Amott wettability index of -0.11 Zou et al. (2018). Full details of the OTS treatment method are available in Kumar et al. (2008).

Relative permeability was measured using the steady-state method ( $Ca = 7.8 * 10^{-6}$ ), as explained by McPhee et al. (2015). The Capillary end effect was accounted for by history



matching the steady-state data. An independently measured capillary pressure versus saturation curve, porosity, and absolute permeability were used as known values for the history matching. Saturation profiles along the core were determined from micro-CT images of the core at each steady-state condition. The core was initially saturated with water followed by a co-injection of water and oil under a drainage sequence. The applied factional flows were 0.9, 0.5, 0.1 and 0. The fractional flow is defined as  $F_w = Q_w/(Q_w + Q_n)$ , where  $Q_w$  is the volumetric flow rate of the wetting phase and  $Q_n$  is the volumetric flow rate of the non-wetting phase.

#### 3 Results and Discussion

Firstly, we will present the relative permeability curves used for our analyzes. We then present the co-moving velocity relationships using the method presented in Sect. 2.1. Lastly, we present a method to predict the relative permeability of the oil phase based on a simplified co-moving velocity relationship and the relative permeability of the water phase.

## 3.1 Effective Permeability Curves

All of the tested data are shown in Fig. 1. Although these data have been published elsewhere (McClure et al. 2021; Zou et al. 2018; Al-Zubaidi et al. 2023) the curves are presented herein to provide a comparison to the co-moving velocity plots in the following subsection. Instead of plotting relative permeability, we plot the effective permeability of each phase,

$$K_{\text{eff}} = K_{ri} \mathsf{K},$$
 (15)

versus saturation. In total, we have 41 effective permeability curves for the North Sea sandstone domain, 5 effective permeability curves for the Bentheimer sandstone domain, and 2 experimentally measured effective permeability curves for Bentheimer sandstone. For all data, the effective permeability curves demonstrate the classic trend in which the effective relative permeability of oil increases as the rock becomes more water wet, while the permeability of the water phase decreases Owens and Archer (1971).

The North Sea sandstone simulations (Fig. 1a) were performed at a Capillary number of approximately  $10^{-5}$ , which is commonly considered the transition point between capillary-dominated to viscous-dominated flow. At this transition, the effective permeability curves were impacted by the wetting state; e.g., under viscous dominant conditions, the effective permeability curves would be straight lines. Furthermore, Al-Zubaidi et al. (2023) shows that a wide range of different geometrical states are present in the North Sea simulations. A similar behavior is observed for the Bentheimer sandstone simulations (Fig. 1b). Overall, the impact of wettability results in different seepage velocities for each phase for a given pressure gradient, which will be mapped to the seepage velocity and co-moving velocity reference frame in the following subsection.

The Bentheimer sandstone experiments (Fig. 1c) demonstrate a change in wettability due to the OTS treatment of the sample. Zou et al. (2018) reports an Amott wettability index of 0.72 for the water-wet case and -0.11 for the mixed-wet case. The observed change in the effective permeability curves is consistent with the trend observed in the simulation results in Fig. 1a, b. The core flooding experiment was conducted with the core initially fully saturated with water, which explains why the effective permeability of the water



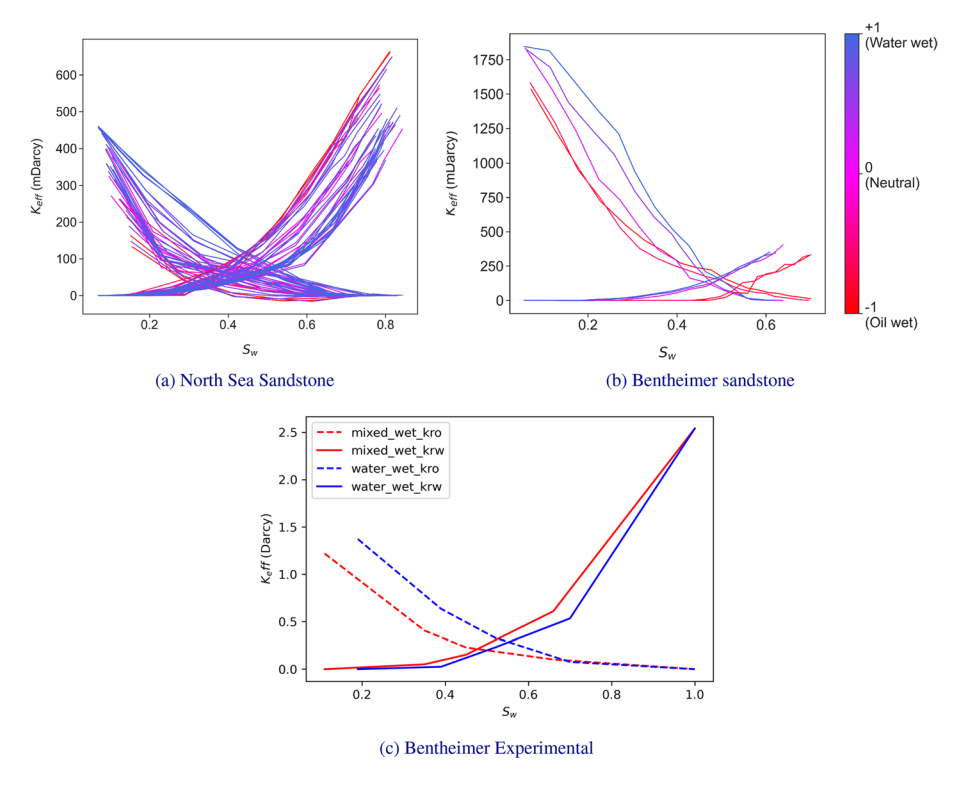


Fig. 1 Relative permeability curves for a range of different wetting conditions. a and b are based on simulation data. c Is experimentally measured steady-state relative permeability

phase at  $S_w = 1$  is reported. Simulations of Bentheimer sandstone were conducted under water flooding, resulting in residual oil saturation, and thus a lower effective end-point permeability for water than that observed in the experimental data. Although these details are important for understanding the reported effective permeability curves, the underlying theory that will be applied to the data (in the following subsection) is only concerned with the relationship between the seepage velocities of each phase.

## 3.2 Co-moving Velocity Relationship

The derived correlations for the North Sea data are presented in Fig. 2, see also Fig. 3. The results indicate that  $v_p/v_0$  versus  $S_w$ , and  $v_m/v_0$  versus  $S_w$  varied between the different wetting conditions. In general, the curves shifted toward the right (higher  $S_w$ ) for more water-wet cases, which is due to their associated effective permeability curves that also exhibit a similar trend for more water-wet conditions. In addition, for a single curve, it can be observed that the global minimum in  $v_p/v_0$  versus  $S_w$  corresponds to the minimum of the total phase mobility. Minimum total seepage velocity occurs when the total mobility of



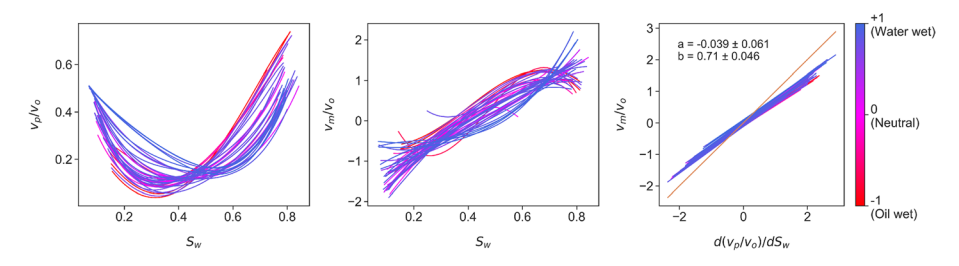


Fig. 2 Derived relationships for the North Sea sandstone based on 41 different wetting conditions

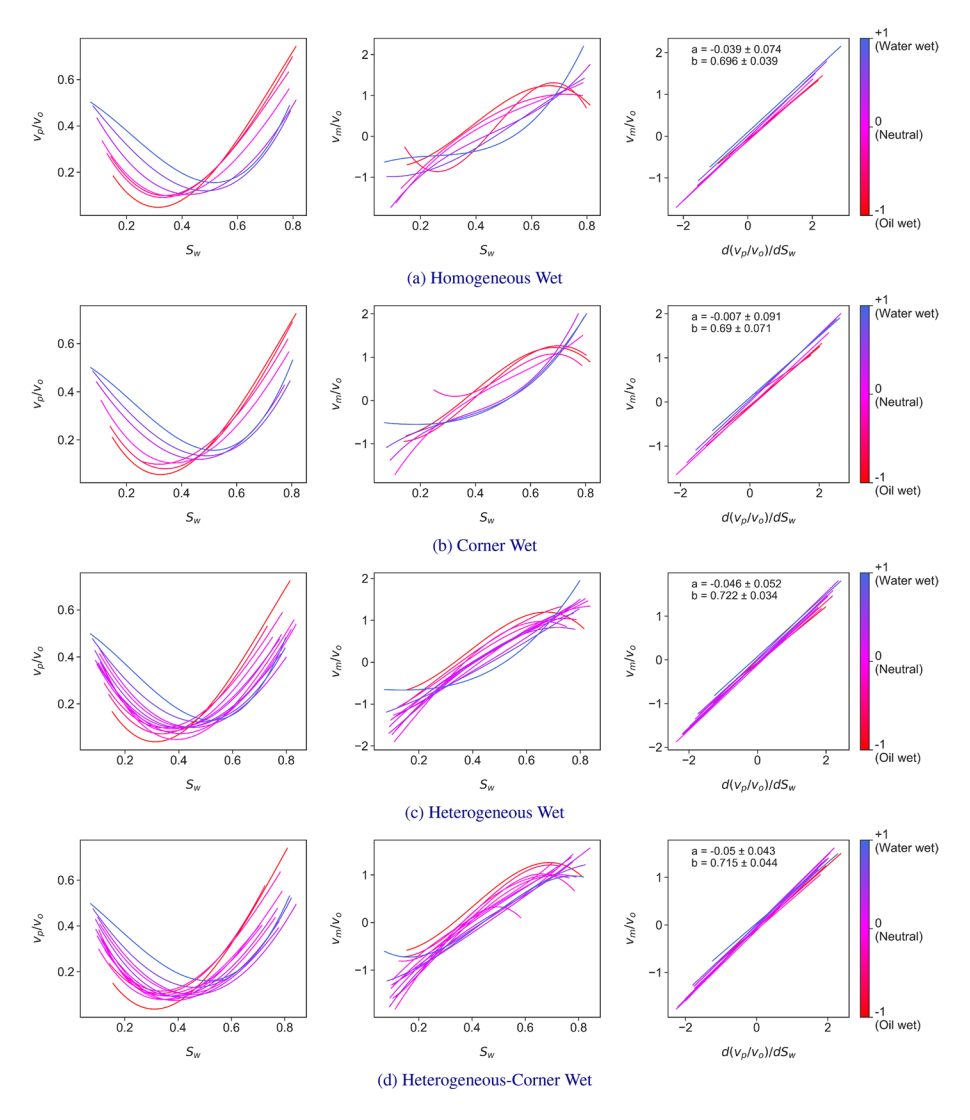


Fig. 3 Derived correlations for North Sea Sandstone with results for each wetting condition



both phases is minimum. Remarkably,  $v_m/v_0$  versus  $d(v_p/v_0)/dS_w$  provided a linear relationship that was nearly the same for all wettability conditions. The linear relationship was consistent for 40 of the 41 different wetting states tested.

The derived correlations for the Bentheimer sandstone simulations are presented in Fig. 4. Overall, the relationships  $v_p/v_0$  versus  $S_w$ , and  $v_m/v_0$  versus  $S_w$  varied to those observed for the North Sea sandstone. However, as observed with the North Sea sample, the linear relationship between  $v_m/v_0$  and  $d(v_p/v_0)/dS_w$  was not influenced by the wetting condition. These results confirm with an independent sample that wettability has little to no effect on the linear relationship for the co-moving velocity.

The derived correlations for the Bentheimer sandstone experimental measurements are presented in Fig. 5. As observed with both simulation data sets, the wetting condition had little to no effect on the linear relationship between  $v_m/v_0$  and  $d(v_p/v_0)/dS_w$ . These results confirm that the observed consistent linear relationship is of physical origin and is not caused by the numerical method implemented in the previous simulation results.

The average coefficients a and b for the simulated North Sea and Bentheimer sandstone samples are reported in Table 1. A full list of coefficients for the North Sea sandstone simulations is provided in Table 2 of the Appendix. Given the standard deviations of the coefficients, the coefficient values for both rock samples are similar. In fact, the samples were also similar in terms of permeability and porosity, in addition to both samples being sandstone. It appears that the differences in rock structure for these samples were not strong enough to

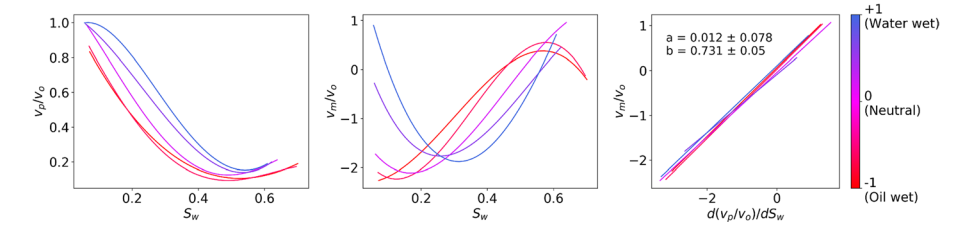


Fig. 4 Derived correlations for Bentheimer sandstone with results from 5 different wetting conditions

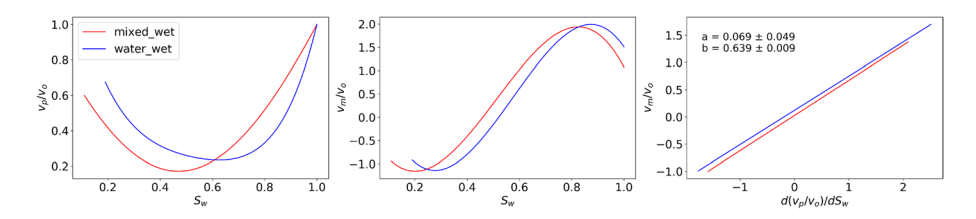


Fig. 5 Derived correlations based on the Bentheimer steady-state experimentally measured relative permeability data

**Table 1** Coefficients *a* and *b* for the co-moving velocity relationship

	а	b
North Sea sandstone	$-0.039 \pm 0.061$	$0.71 \pm 0.046$
Bentheimer sandstone	$0.012 \pm 0.078$	$0.731 \pm 0.050$

The reported coefficients are the average for all simulated wetting states and associated errors are based on the standard deviation



clearly observe any discernible differences in the co-moving velocity relationship. Roy et al. (2022) analyzed relative permeability data form a wider range of different rocks, fluids, and flow rates, which provided more variability in coefficient values than that observed in our data. The limited range of values observed in our data is likely due the limited impact of wettability on the co-moving velocity.

The impacts of Capillary number and mobility ratio on coefficients a and b were explored in Roy et al. (2022) using a dynamic pore network model. While b increased with Capillary number, a appeared to approach zero. Furthermore, for an intermediate range of mobility ratios, both a and b increased with mobility ratio, while at higher and lower mobility ratios there was no influence on a and b. The influence of wettability was not explored by Roy et al. (2022) yet the reported experimental data provided coefficient values (a and b) within a similar range of the values presented in Tables 1 and 2 of the Appendix.

## 3.3 Effective Permeability Prediction

An essential result of this work is that wettability had limited influence on the co-moving velocity relationship. Therefore, once this relationship is known, it can be applied to any given wetting case in the same rock.

To simplify the co-moving velocity relationship, we propose

$$v_m = b \frac{dv_p}{dS_w},\tag{16}$$

given that *a* was nearly zero for all tested cases. This provides a condition (or constraint) on how one relative permeability curve must change in relation to another. This symmetry relation based on our results appears to be true for different wetting conditions in the same rock. Therefore, given one relative permeability curve and *b* for Eq. 16, the other paired relative permeability curve can be predicted. This we see from Eqs. 9 and 10: knowing one of the relative permeabilities, we can turn these two equations into a differential equation for the other.

In the following, we proceed along a path that does not require the solving of a differential equation. We start with a Corey relationship for the effective permeability of the oil phase with an unknown Corey exponent,  $\eta_o$ . This Corey relationship is paired with the simulated known water phase effective permeability. The co-moving velocity relationship can then be determined using these paired data (using the approach explained in Sect. 2) to provide  $b_{\text{predict}}$ . We then search  $\eta_o$  over a reasonable range of Corey exponents (1 to 10) to find min  $|b_{\text{predict}} - b_{NS}|$ , where  $b_{NS}$  is the average coefficient value (b) for the North Sea data (see Table 1).

Six simulation cases from the North Sea Sandstone data that span the entire range of simulated wettabilities are presented in Fig. 6. For each case, the predicted oil phase relative permeability curves are nearly equivalent to the actual simulation data. The wettability index, W, is reported for each case tested. The prediction error is likely associated with two factors. (1) The co-moving velocity relationship was simplified by considering a y-intercept of zero for the general model. (2) The maximum effective permeability of the oil phase,  $k_{rn,max} = 1$ , was assumed to be constant for all cases.  $k_{rn,max}$  could indeed be used as an additional fitting parameter, but our aim was to demonstrate the simplest approach possible.



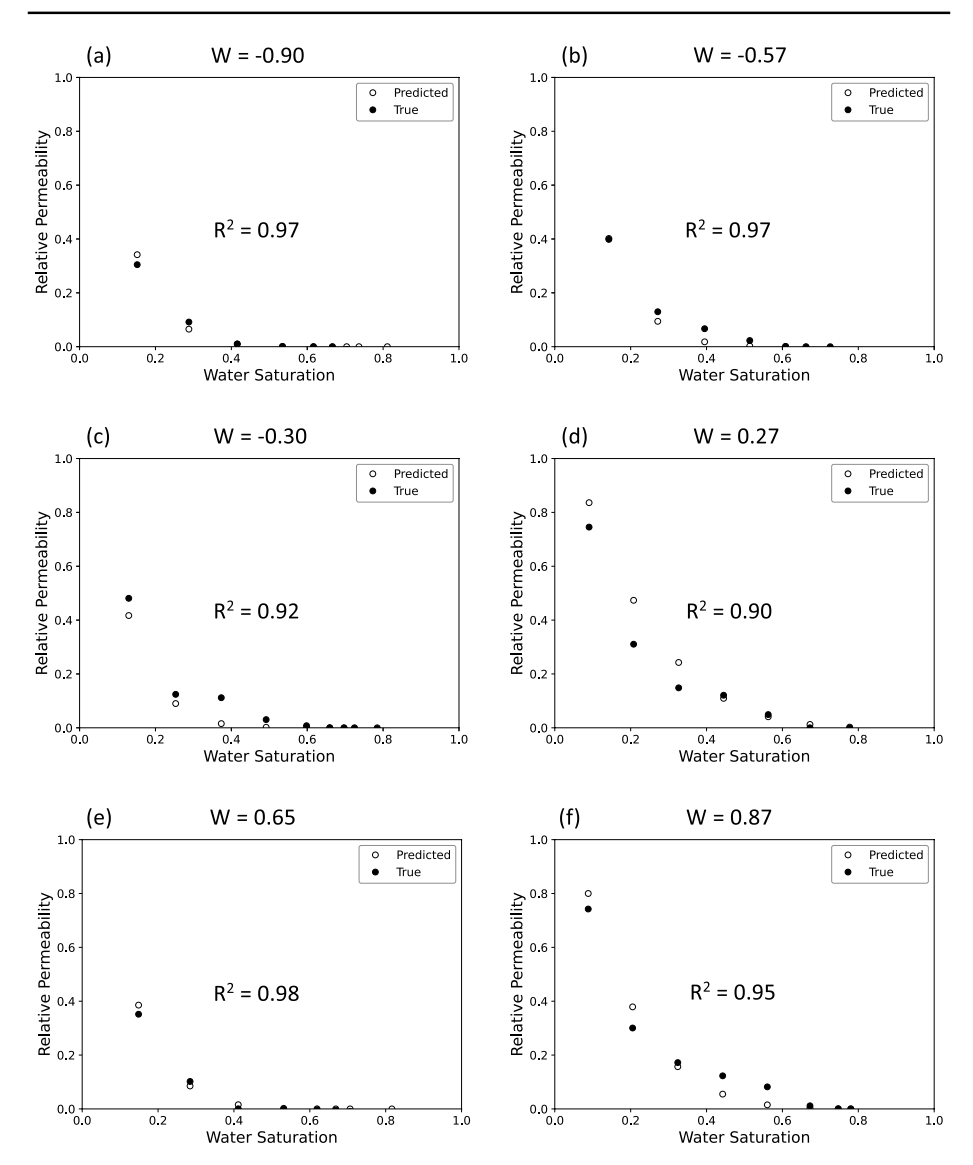


**Fig. 6** Predicted versus true effective permeability curves for the oil phase. Predictions are based on the simulated water phase effective permeabilities and a single average co-moving velocity relationship for the North Sea sandstone

## 4 Conclusion

Our main result is that the co-moving velocity relationship remains linear for all the tested wetting conditions. In addition, the wetting state had little to no effect on the coefficients for the co-moving velocity relationship even though the relative permeability



was significantly affected by the wetting state. Our results were consistent for both the experimental and the simulation data. Other works have also reported a simple affine form for the co-moving velocity based on pore network modeling Roy et al. (2022). However, our work differs from previous work by two factors. (1) We demonstrate consistent behavior for all wetting states. (2) We demonstrate a workflow to predict complete relative permeability curves when only one set of relative permeabilities is measured and the co-moving velocity relationship is known. In future work, the extent to which the coefficients (a and b) for Eq. 6 differ under different Capillary numbers, mobility ratios, and hysteric cycles should be explored experimentally, since current results are limited to dynamic pore network modeling in Roy et al. (2022). Given our current results, we would expect the same coefficients (a and b) for a given rock under different wetting conditions at low Capillary number flows ( $10^6$  to  $10^5$ ).

On the basis of our results, new laboratory workflows can be envisaged when determining the relative permeability curves of a rock core under different wetting conditions. A specific example would be the case of determining relative permeability from the single-speed centrifuge method McPhee et al. (2015) where only the relative permeability curve of the least dense phase is measured. Having a methodology, such as the one presented herein, to determine the relative permeability of the other phase would be beneficial. Although you still need a full set of relative permeability curves to determine the coefficients (a and b), our results demonstrate that different wettabilities provide the same (a and b) for a given sample. Once (a and b) are determined for a sample, subsequent studies could be conducted with fast experimental protocols, such as the centrifuge method, without the limitation of providing only the relative permeability of the least dense phase.

In addition, the universality of the linear relationship for the co-moving velocity is a remarkable result. The total seepage velocity and the co-moving velocity are a coupled pair that contain the same information as the coupled wetting and non-wetting seepage velocities, i.e.,  $(v_p, v_m) \leftrightarrow (v_w, v_n)$ . Therefore, relative permeability within the traditional two-phase extension of Darcy's law could be determined by measuring only the total seepage velocity and average pressure gradient when the co-moving velocity relationship is known for a given rock type. Potentially, history matching approaches used to determine relative permeability could benefit from the additional constraint provided by the co-moving velocity relationship, since it links the behavior of the two relative permeability curves. The usage of the co-moving velocity relationship for the history matching of core flooding data Lenormand and Lenormand (2016) would be an interesting topic for future work.

Overall, our results show that the representation of two-fluid flow based on the co-moving velocity is simpler and more universal than expected. This suggests that our alternative representation may have advantages with respect to the conventional representation.

## **Appendix**

A full list of coefficients *a* and *b* for the North Sea sandstone simulations is provided in Table 2. The average and standard deviation reported in Table 1 are based on the values reported in Table 2.



**Table 2** Coefficients a and b for the co-moving velocity relationship, and the domain wettability W as given by Eq. (14)

Wetting condition	W	а	b
	0.900	0.096	0.712
	0.600	0.019	0.709
	0.300	-0.044	0.750
Homogeneous wet	0.000	- 0.097	0.726
	-0.300	-0.117	0.683
	-0.600	- 0.066	0.654
	-0.900	-0.065	0.642
	0.981	0.098	0.696
	0.925	0.047	0.731
	0.869	0.005	0.761
Corner wet	0.813	-0.097	0.732
	0.757	0.095	0.546
	0.701	-0.118	0.697
	0.646	-0.081	0.663
	0.962	0.076	0.71
	0.912	-0.004	0.709
	0.870	-0.064	0.747
	0.811	-0.115	0.744
	0.766	-0.095	0.68
Heterogeneous wet	0.707	-0.076	0.703
	0.634	- 0.059	0.638
	0.832	0.019	0.759
	0.804	- 0.012	0.726
	0.784	- 0.064	0.743
	0.822	-0.064	0.76
Heterogeneous-Corner wet	0.842	- 0.059	0.737
	0.817	-0.079	0.724
	0.807	0.035	0.639
	0.527	-0.007	0.701
	0.267	-0.04	0.761
	- 0.026	- 0.117	0.734
	- 0.249	-0.102	0.646
	-0.574	-0.07	0.676
	- 0.939	-0.066	0.661
	0.142	0.006	0.738
	-0.028	-0.003	0.736
	-0.177	-0.071	0.749
	-0.021	-0.046	0.778
	0.139	-0.07	0.741
	-0.014	-0.074	0.725
	-0.107	-0.071	0.731



**Acknowledgements** R. T. A. acknowledges Australian Research Council Future Fellowship (FT210100165) and Discovery (DP210102689). This work was furthermore supported by the Research Council of Norway through its Center of Excellence funding scheme, project number 262644 (HP, AH and CFB). This research used resources of the Oak Ridge Leadership Computing Facility, which is a DOE Office of Science User Facility supported under Contract DE-AC05-00OR22725.

Funding Open Access funding enabled and organized by CAUL and its Member Institutions.

Data Availability The relative permeability data and code used for reverse engineering is available at https://github.com/fatimahgit via DOI 10.5281/zendo.8322537.

Open Access This article is licensed under a Creative Commons Attribution 4.0 International License, which permits use, sharing, adaptation, distribution and reproduction in any medium or format, as long as you give appropriate credit to the original author(s) and the source, provide a link to the Creative Commons licence, and indicate if changes were made. The images or other third party material in this article are included in the article's Creative Commons licence, unless indicated otherwise in a credit line to the material. If material is not included in the article's Creative Commons licence and your intended use is not permitted by statutory regulation or exceeds the permitted use, you will need to obtain permission directly from the copyright holder. To view a copy of this licence, visit http://creativecommons.org/licenses/by/4.0/.

## References

- Al-Zubaidi, F., Mostaghimi, P., Niu, Y., Armstrong, R.T., Mohammadi, G., McClure, J.E., Berg, S.: Effective permeability of an immiscible fluid in porous media determined from its geometric state. Phys. Rev. Fluids 8, 064004 (2023). https://doi.org/10.1103/PhysRevFluids.8.064004
- Anderson, W.G.: Wettability literature survey-part 1: rock/oil/brine interactions and the effects of core handling on wettability. J. Petrol. Technol. 38(10), 1125–1144 (1986)
- Anderson, W.G.: Wettability literature survey part 5: the effects of wettability on relative permeability. J. Petrol. Technol. 39(11), 1453–1468 (1987)
- Armstrong, R.T., McClure, J.E., Robins, V., Liu, Z., Arns, C.H., Schlüter, S., Berg, S.: Porous media characterization using minkowski functionals: theories, applications and future directions. Transp. Porous Media 130, 305–335 (2019)
- Armstrong, R.T., Sun, C., Mostaghimi, P., Berg, S., Rücker, M., Luckham, P., Georgiadis, A., McClure, J.E.: Multiscale characterization of wettability in porous media. Transp. Porous Media **140**(1), 215–240 (2021)
- Feder, J., Flekkøy, E.G., Hansen, A.: Physics of Flow in Porous Media. Cambridge University Press, Cambridge (2022)
- Garfi, G., John, C. M., Lin, Q., Berg, S., Krevor, S.: Fluid surface coverage showing the controls of rock mineralogy on the wetting state. *Geophys. Res. Lett.*, 47(8):e2019GL086380 (2020)
- Hansen, A., Sinha, S., Bedeaux, D., Kjelstrup, S., Gjennestad, M.A., Vassvik, M.: Relations between seepage velocities in immiscible, incompressible two-phase flow in porous media. Transp. Porous Media 125(3), 565–587 (2018)
- Hansen, A., Flekkøy, E.G., Sinha, S., Slotte, P.A.: A statistical mechanics framework for immiscible and incompressible two-phase flow in porous media. Adv. Water Resour. 171, 104336 (2023)
- Kumar, M., Senden, T., Latham, S., Sheppard, A., Knackstedt, M. A., Cinar, Y., Pinczewski, W. V.: Designing for mixed wettability. In SPE Improved Oil Recovery Conference?, pp. SPE–113862. SPE (2008)
- Lenormand, R., Lenormand, G.: Recommended procedure for determination of relative permeabilities. In: International Symposium of the Society of Core Analysts held in Snowmass, Colorado, USA, pp. 21–26 (2016)
- Lin, Q., Bijeljic, B., Pini, R., Blunt, M.J., Krevor, S.: Imaging and measurement of pore-scale interfacial curvature to determine capillary pressure simultaneously with relative permeability. Water Resour. Res. 54(9), 7046–7060 (2018)
- Lin, Q., Bijeljic, B., Berg, S., Pini, R., Blunt, M.J., Krevor, S.: Minimal surfaces in porous media: Pore-scale imaging of multiphase flow in an altered-wettability bentheimer sandstone. Phys. Rev. E 99(6), 063105 (2019)
- Lin, Q., Bijeljic, B., Foroughi, S., Berg, S., Blunt, M.J.: Pore-scale imaging of displacement patterns in an altered-wettability carbonate. Chem. Eng. Sci. 235, 116464 (2021)



Masalmeh, S.K.: The effect of wettability heterogeneity on capillary pressure and relative permeability. J. Petrol. Sci. Eng. 39(3-4), 399-408 (2003)

- McClure, J.E., Armstrong, R.T., Berrill, M.A., Schlüter, S., Berg, S., Gray, W.G., Miller, C.T.: Geometric state function for two-fluid flow in porous media. Phys. Rev. Fluids 3(8), 084306 (2018)
- McClure, J.E., Li, Z., Berrill, M., Ramstad, T.: The lbpm software package for simulating multiphase flow on digital images of porous rocks. Comput. Geosci. 25(3), 871–895 (2021)
- McPhee, C., Reed, J., Zubizarreta, I.: Preparation for special core analysis. In: Developments in Petroleum Science, Vol. 64, pp. 269–312. Elsevier (2015)
- Owens, W., Archer, D.: The effect of rock wettability on oil-water relative permeability relationships. J. Petrol. Technol. 23(07), 873–878 (1971)
- Pedersen, H., Hansen, A.: Parameterizations of immiscible two-phase flow in porous media. Front. Phys. 11, 116 (2023)
- Reynolds, C.A., Menke, H., Andrew, M., Blunt, M.J., Krevor, S.: Dynamic fluid connectivity during steadystate multiphase flow in a sandstone. Proc. Natl. Acad. Sci. 114(31), 8187–8192 (2017)
- Roy, S., Sinha, S., Hansen, A.: Flow-area relations in immiscible two-phase flow in porous media. Front. Phys. 8, 4 (2020)
- Roy, S., Pedersen, H., Sinha, S., Hansen, A.: The co-moving velocity in immiscible two-phase flow in porous media. Transp. Porous Media 143(1), 69–102 (2022)
- Scanziani, A., Lin, Q., Alhosani, A., Blunt, M.J., Bijeljic, B.: Dynamics of fluid displacement in mixed-wet porous media. Proc. R. Soc. A 476(2240), 20200040 (2020)
- Wyckoff, R., Botset, H.: The flow of gas-liquid mixtures through unconsolidated sands. Physics 7(9), 325–345 (1936)
- Zou, S., Armstrong, R.T., Arns, J.-Y., Arns, C.H., Hussain, F.: Experimental and theoretical evidence for increased ganglion dynamics during fractional flow in mixed-wet porous media. Water Resour. Res. 54(5), 3277–3289 (2018)

**Publisher's Note** Springer Nature remains neutral with regard to jurisdictional claims in published maps and institutional affiliations.

